Room-Temperature O3 detection: zero-bias sensors based on ZnO thin films

Eleonora Bolli *, Alice Fornari, Alessandro Bellucci, Matteo Mastellone, Veronica Valentini, Alessio Mezzi, Riccardo Polini, Antonio Santagata, Daniele Maria Trucchi

Posted Date: 15 December 2023

doi: 10.20944/preprints202312.1121.v1

Keywords: thin film; MOS; gas sensor; chemiresistor

Article

Room-Temperature O_3 Detection: Zero-Bias Sensors Based on ZnO Thin Films

Eleonora Bolli [1,*], Alice Fornari [1], Alessandro Bellucci [1], Matteo Mastellone [2], Veronica Valentini [1], Alessio Mezzi [3], Riccardo Polini [4], Antonio Santagata [2] and Daniele Maria Trucchi [1]

[1] CNR-ISM, DiaTHEMA Lab, U.O.S. Montelibretti, Via Salaria km 29.300, 00015 Monterotondo, Italy
[2] CNR-ISM, FemtoLAB, U.O.S. Tito Scalo, Zona Industriale, 85050 Tito, Italy
[3] CNR-ISMN, EscaLab, Montelibretti, Via Salaria km 29.300, 00015 Monterotondo, Italy
[4] Dipartimento di Scienze e Tecnologie Chimiche, Università di Roma 'Tor Vergata', 00133 Rome, Italy
* Correspondence: eleonora.bolli@ism.cnr.it;

Abstract: ZnO thin films with a thickness of 300 nm were deposited on Si and Al_2O_3 substrates using electron beam evaporation technique with the aim to be tested as low cost and low power consumption gas sensors for ozone (O_3). To characterize the surface roughness and the grain size, which are the main parameters recognized to enhance gas sensitivity since they directly influence the effective sensing area, surface morphology and roughness analyses of the films were performed using scanning electron microscopy and atomic force microscopy, respectively. The crystalline structure and elemental composition were studied through Raman spectroscopy and X-ray photoelectron spectroscopy. Gas tests were conducted at room temperature and zero-bias voltage to assess the sensitivity and response as a function of time of the films to O_3 pollutant. The results indicate that the films deposited on Al_2O_3 exhibit promising characteristics, such as high sensitivity and a very short response time (< 2 s) to the gas concentration. Additionally, it was observed that the films display pronounced degradation effects after a significant exposure to O_3.

Keywords: thin film; MOS; gas sensor; chemiresistor

1. Introduction

The increasing demand for monitoring air pollution, particularly due to greenhouse gases like CO_2, NO_2, SO_2, and O_3 [1] is a current challenge for human health care and environmental application.

According to the World Health Organization's air quality guideline for ozone [2], it is recommended that daily exposure to ozone, ensuring sufficient protection of human health, should not exceed 100 μg/m³, approximately equivalent to 50 parts per billion (ppb), as a maximum 8-hour mean concentration. Since people spend most of their time in environments such as residences, schools and offices, it is crucial to pay attention to indoor ozone exposure. Despite average ozone concentration levels in these spaces range from 4-6 ppb [3], peak concentrations during the day could exceed the WHO reference values [3].

Nowadays, the development of advanced gas sensors is fundamental to real-time monitor the ozone concentration in indoor environments.

This latest generation of solid-state gas sensors reflects a transition from bulk materials with good intrinsic properties to materials with size- and shape-dependent surface properties, including nanostructured materials, nanoparticles, and ultra-thin films [4–6]. Thin films offer functionalized surfaces suitable for a wide range of applications [7–9], by combining different parameters such as thickness, substrate employed, and deposition method used. With an increased surface-to-volume ratio, nanostructured thin films exhibit good performance in terms of sensitivity, selectivity, and quick response time [10–12].

Furthermore, the reduced size of thin films enables low-cost production processes and easy integration into devices, allowing for constant remote monitoring, wireless data collection, and processing using plug and play IoT (Internet of Things) technologies [13,14].

 doi:10.20944/preprints202312.1121.v1

Thin film gas sensors can be made using both metal and metal oxide semiconductors (MOSs). MOS sensors based on SnO_2, ZnO, CuO, and WO_3 are particularly interesting for their high surface sensitivity and stability [15–19]. When exposed to gas, MOSs exhibit a chemiresistor behavior, where the electronic properties change upon gas molecule adsorption, enabling the detection of harmful gases through variation in the electrical resistivity [20].

While MOSs-based gas sensors exhibit very short response times, high operating temperatures (300-500 °C) are typically required to achieve optimal sensitivity conditions [5,20–22]. However, ZnO can operate at lower temperatures and it has been demonstrated that ZnO thin films can maintain high sensitivity even at lower temperatures (< 100 °C down to room temperature) by optimizing film parameters such as grain size and porosity [5,24,25].

The choice of the physical vapor deposition (PVD) technique during the growth phase, such as magnetron sputtering, pulsed laser deposition (PLD), and electron-beam deposition, allows for control of these parameters. Each PVD technique offers respective advantages: magnetron sputtering enables higher thickness control, which is useful for ultra-thin film deposition [26]; PLD, on the other hand, guarantees higher ZnO crystallinity [26]. However, a recent study has suggested that electron-beam deposition is the most suitable technique for gas sensor design, as it generates polycrystalline films with high surface area [26].

Different deposition methods yield ZnO films with varying grain sizes. The porosity, indeed, can be induced by growing the film on a rough substrate. Therefore, as a direct consequence of enhancing the surface to bulk ratio, it has been demonstrated that gas sensors require a porous microstructure as well as their sensitivity considerably increases as grain size decreases [27,28].

This study aims to investigate the possibility of fabricating ZnO thin films that are suitable to operate at room temperature with good sensitivity. To achieve this, ZnO thin films were deposited by using electron beam deposition on Si and Al_2O_3 substrates and by optimizing the growth conditions.

First, the substrate was selected by studying the morphology and surface roughness of the deposited ZnO thin films, using scanning electron microscopy and atomic force microscopy.

Then, the structural and elemental analysis of the films were characterized by Raman and X-ray Photoelectron (XPS) spectroscopies, respectively. The ZnO-based sensors were exposed to O_3 gas for sensitivity testing. In addition to analyzing the variation of electrical properties, the effects of O_3 gas exposure on the film surfaces were also studied to verify the induced effects onto the surface.

2. Materials and Methods

2.1. Films Depositions by Electron Beam Evaporation

Thin films of ZnO were deposited by electron beam deposition on silicon wafers and alumina substrates. The deposition was performed in a high vacuum chamber at a base pressure of ~1.0 x 10^{-6} mbar until ~1.0 x 10^{-5} mbar under evaporation with the beam controlled by an electromagnetic lens system to homogenize the deposition process. The ZnO pellets (99.99 % purity, Mateck Material-Technologie & Kristalle GmbH, Julich, Germany) were kept in a molybdenum crucible (Kurt J. Lesker Company GmbH, Dresden, Germany) and heated by an electron beam of 6.5 keV kinetic energy and 18 mA current. Those parameters lead to film of 300 nm thickness after 5 minutes of deposition (the deposited film thickness was verified using atomic force microscope profiles). The deposition rate of about 1 nm/s was constantly monitored by in-situ quartz microbalance.

2.2. Structure and Morphology Characterization

The morphology of the ZnO thin films has been investigated by Field-Emission Gun Scanning Electron Microscopy (FEG-SEM- Zeiss Leo Supra 35, Germany) and by Atomic Force Microscopy (AFM) carried out with use of an OmegaScope platform (HORIBA Ltd., Kyoto, Japan). AFM imaging was performed in tapping mode, setting the operational amplitude at 60 nm, and using a silicon pyramidal tip (MikroMasch HQ:NSC14/Al BS; Wetzlar, Germany) with a characteristic radius of ~8 nm. The resonance frequency was of 137 kHz. The scan rate was fixed at 0.6 Hz. All the AFM data

Preprints (www.preprints.org) | NOT PEER-REVIEWED | Posted: 15 December 2023 doi:10.20944/preprints202312.1121.v1

were acquired, filtered, and analyzed using the AIST-NT SPM control software. Raman measurements were carried out by using a Horiba Scientific LabRam HR Evolution confocal spectrometer equipped with a 100mW Oxxius (λ_{exc} = 532 nm) and 17mW He-Ne (λ_{exc} = 633 nm) laser sources and a computerized XY-table, an electron-multiplier CCD detector, an Olympus U5RE2 microscope with a 100x objective (laser spot on the sample surface 0.7 μm) with a numerical aperture (NA) of 0.9, and a grating with 1800 grooves/mm. All Raman spectra were recorded in backscattering geometry focusing 10% of the laser sources power at the sample and twenty spectra with an accumulation time of 10 s were averaged. Samples were measured before and after the gas exposure. XPS provides to investigate the composition of the ZnO films and it was carried out by using a spectrometer ESCALAB 250 Xi (Thermo Fisher Scientific, UK), equipped with a monochromatic Al Kαsource (hν = 1486.6 eV) and a hemispherical analyzer with six-channeltron as detection system. The XPS characterizations were performed in ultra-high vacuum chamber at a base pressure of about 1 x 10^{-9} mbar. The binding energy (BE) scale was calibrated by positioning the C 1s adventitious carbon peak at BE = 285.0 eV with an accuracy of ±0.1 eV.

2.3. Gas sensing

The gas sensor tests were performed using a commercial glove box (Cole-Parmer Instrument Company, LLC, United Kingdom) with a volume of about 0.25 m^3, suitable to keep the gas concentration confined. Thanks to a customized ozone generator system (IONVAC Process srl, Pomezia, Italy), it was possible to regulate the flow of O_3 in the chamber which is evacuated by a membrane pump (pressure of ~ 10^{-1} mbar) to assure stable conditions and fast removal of ozone. The current measurements were carried out by connecting the sensor to an electrometer (Keithley 487 Picoammeter/Voltage Source), recording the data in an automated way through the management of the signals with the GPIB protocol and a software specifically developed with the LabVIEW (National Instruments) language. The measurements were carried out by observing potential variations in the current flow across the sensor surface in response to different pollutant concentrations inside the glove box.

3. Results and Discussion

ZnO thin films were deposited on Si and alumina substrates by applying the declared deposition parameters to obtain homogenous and continuous thin films. To achieve this, we found that the best conditions were to maintain a deposition rate of 1 nm/s and to fix a thickness of 300 nm. Figure 1 illustrates the morphological differences between the films grown on Si (Figure 1a) and on alumina (Figure 1b) under the same conditions. The film deposited on Si appears smoother compared to the film grown on alumina The average grain size was found to be 53 ± 13 nm for the Si-deposited film and 24 ± 5 nm for the alumina-deposited film.

Furthermore, atomic force microscopy (AFM) analysis, as shown in Figure 2, confirmed the smoother surface of the film deposited on Si compared to the film grown on alumina. The roughness parameters R_a and R_{RMS} (i.e., R_a, the arithmetic average of the absolute values of the profile height deviations from the mean line and R_{RMS}, the root mean

square average of the profile height deviations from the mean line) of the films were estimated using Aist software, analyzing images of approximately 25 μm^2 area with a lateral resolution of 500 × 500 pixels (Figure 2a,b). The results of the roughness analysis are summarized in Table 1.

Table 1. Roughness parameters: comparison between R_a and R_{RMS} for bare substrates of Si and Al_2O_3 and ZnO thin films deposited on the two different substrates.

	Si	Al_2O_3	ZnO on Si	ZnO on Al_2O_3
R_a (nm)	3.7	62.3	10.3	61.2
R_{RMS} (nm)	5.4	78.1	12.8	75.5

Preprints (www.preprints.org) | NOT PEER-REVIEWED | Posted: 15 December 2023 doi:10.20944/preprints202312.1121.v1

We found that the morphology of ZnO films strongly depends on the substrate, with different porosity and grain size that play a significant role in the film properties. Since a higher effective area obtained by small grain size and high roughness is required to obtain better sensor performance [27,28], the morphological analysis led to the selection of alumina as the preferred substrate for growing the films to be used in gas sensitivity tests.

XPS measurements were performed to analyse the chemical composition of the most promising ZnO film. The C1s spectrum revealed the presence of contaminants, including adventitious carbon (C1) at a binding energy (BE) of 285.0 eV and carboxyl groups (C2) at a BE of 288.2 eV, due to exposure to air (XPS survey spectrum is shown in Figure 3). A 30 s-duration ion sputtering process with Ar^+ at 2 keV effectively removed all contaminants from the film surface, as shown in Table 2. XPS analysis confirmed the presence of stoichiometric ZnO films, with a slight excess of Zn observed after Ar^+ cleaning due to the preferential sputtering effect described in the literature [29].

Table 2. XPS quantification of 300 nm thick ZnO film deposited on Al_2O_3 before and after 30 s of Ar^+ ion sputtering.

Nome	BE (eV)	at. % as grown	at. % after 30 s of Ar^+	Bond
C1s – A	285.0	11.2	-	C – C
C1s – B	288.2	2.6	-	C = O
O1s – 1	530.0	30.9	37.8	ZnO
O1s – 2	531.8	13.0	5.9	Zn(OH)2
Zn2p3	1021.5	42.3	56.3	ZnO

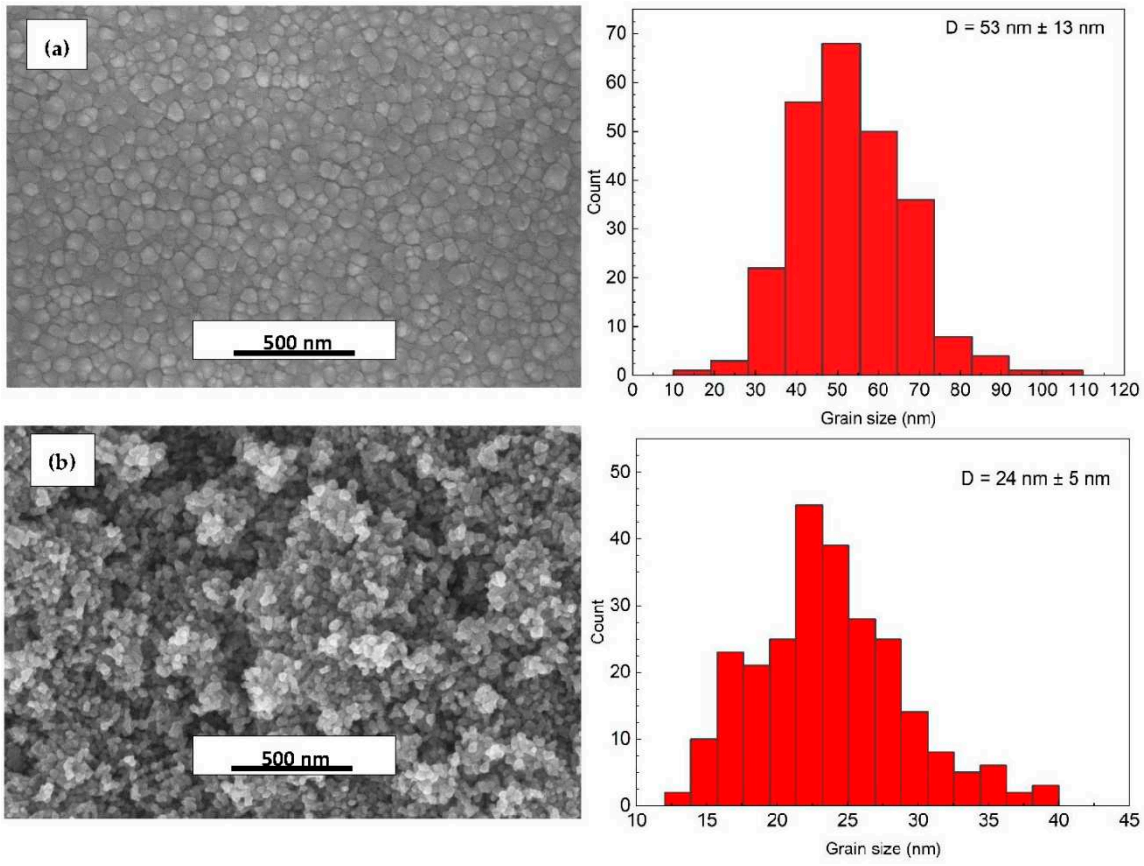

Figure 1. SEM micrographs of ZnO deposited on (**a**) Si and (**b**) Al_2O_3 with corresponding size distribution of crystal's grain diameter D.

Preprints (www.preprints.org) | NOT PEER-REVIEWED | Posted: 15 December 2023 doi:10.20944/preprints202312.1121.v1

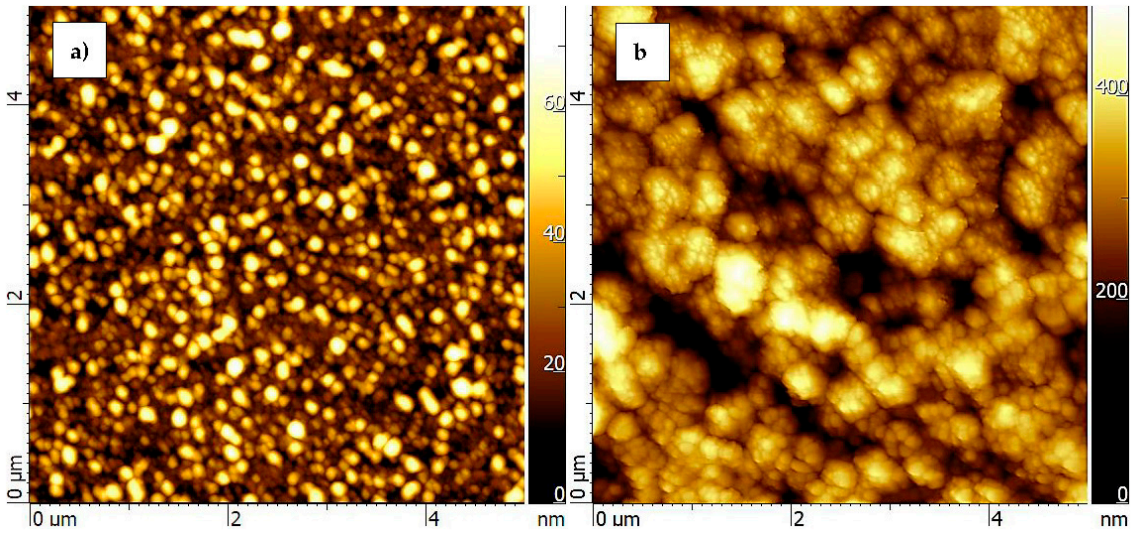

Figure 2. AFM topographies of ZnO films deposited on Si (**a**) and Al_2O_3 (**b**).

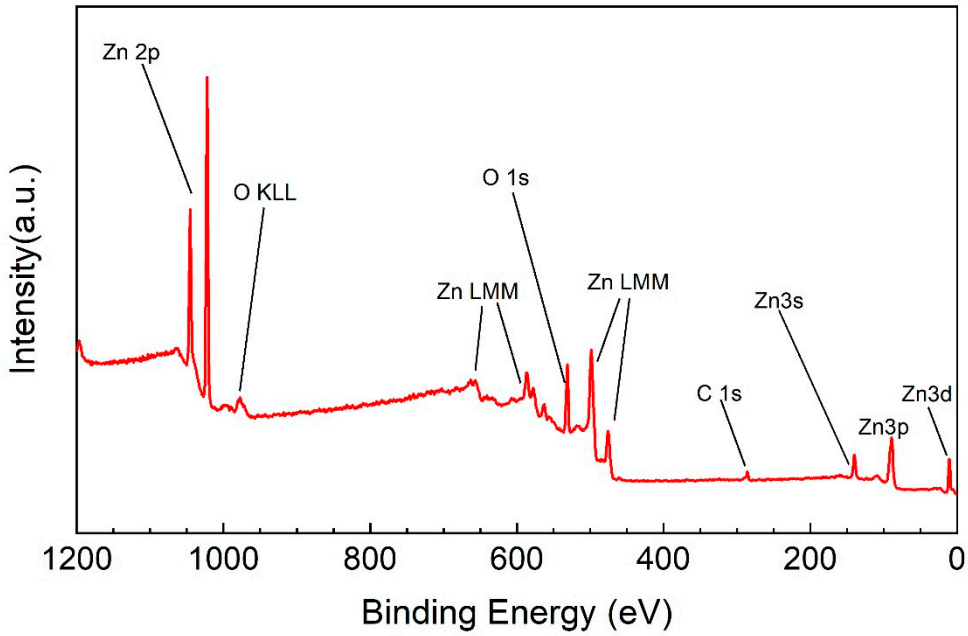

Figure 3. XPS survey spectrum of ZnO film deposited on Al_2O_3 (b).

Raman spectroscopy provided additional information compared to XPS revealing the Al_2O_3 interface. Figure 4a shows the normalized Raman spectrum of the ZnO film deposited on an Al_2O_3 substrate using the excitation wavelength λ_{exc} = 532 nm. The predominant band in the spectrum, centered around 560 cm^{-1}, is attributed to the B1(high) vibration. This vibration, typically silent, can occur in the presence of a cubic structure (zincblende) formed by the growth carried out by e-beam evaporation [30,31]. The band centered at 430-470 cm^{-1}, related to the E2 phonon due to hexagonal wurtzite ZnO, is not observed. The Figure 4b shows the normalized spectrum using the λ_{exc} = 633 nm. Again, the predominant band is centered around 560 cm^{-1} thus confirming the zincblende structure of the film.

Preprints (www.preprints.org) | NOT PEER-REVIEWED | Posted: 15 December 2023 doi:10.20944/preprints202312.1121.v1

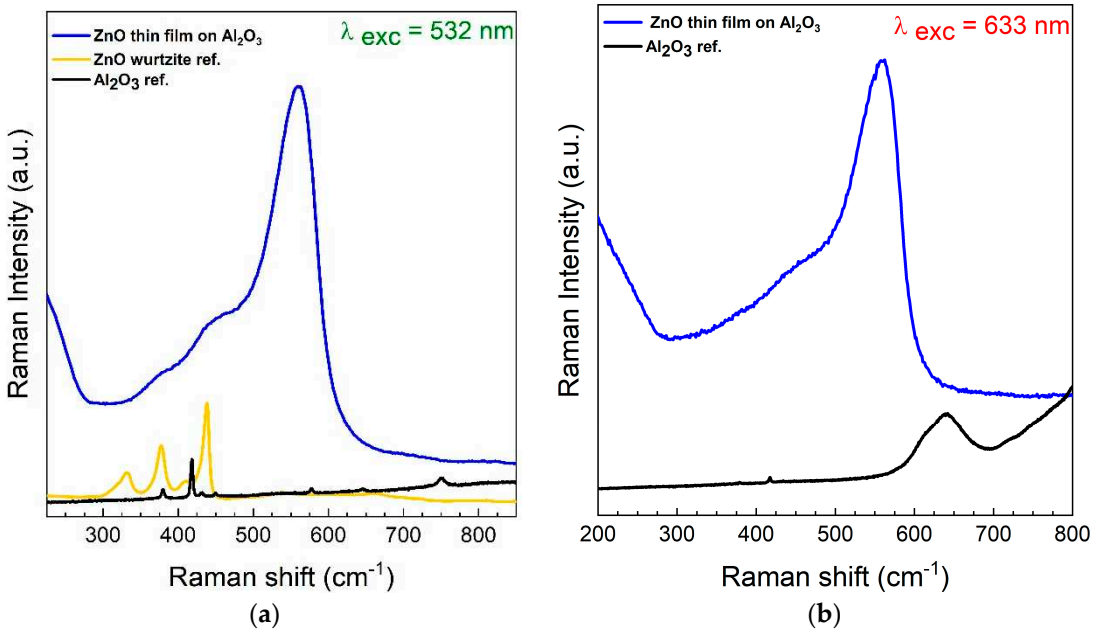

Figure 4. Normalized Raman spectra of a typical ZnO thin film on Al_2O_3 before the exposure to O_3 using λ_{exc} = 532 nm (**a**) and λ_{exc} = 633 nm (**b**) as excitation wavelengths in comparison with ZnO hexagonal wurtzite and Al_2O_3 references. The B1(high) vibration band at ~560 cm^{-1} is due to the presence of cubic zincblende structure.

Following the morphological, structure and elemental composition characterizations, the sensitivity tests were conducted on ZnO thin films deposited by using electron beam deposition on alumina printed-circuit boards produced by CERcuits, Belgium, with Cu/Au metallic contacts.

As described in the Introduction, the focus was on developing a sensor applicable in indoor environments such as schools and offices. For such applications, it is important that the sensor should maintain a low power consumption and minimal maintenance costs. To achieve this, sensitivity tests to ozone were conducted at room temperature (the mechanism of interaction between ZnO and ozone at room temperature was discussed in these previous studies [32,33]) and with zero-bias voltage, aiming to minimize the power consumption. Additionally, it is crucial for the sensor to retain a high sensitivity to the monitored gas even after prolonged exposure to O_3, without the need for frequent replacements. For this reason, a typical test was performed by using the same film through the application of concentrations of O_3 from 50 to 1150 ppb successively by increasing the gas concentration. The response R of the sensor was defined according to the following equation:

$$R = \left| \frac{Igas - Iair}{Iair} \right|$$

where I_{air} and I_{gas} are the electrical currents before and after the O_3 exposure derived from the measured electrical current I_{meas}.

Figure 5 illustrates the response R of the film as a function of the O_3 concentration obtained by applying zero-bias voltage.

Preprints (www.preprints.org) | NOT PEER-REVIEWED | Posted: 15 December 2023 doi:10.20944/preprints202312.1121.v1

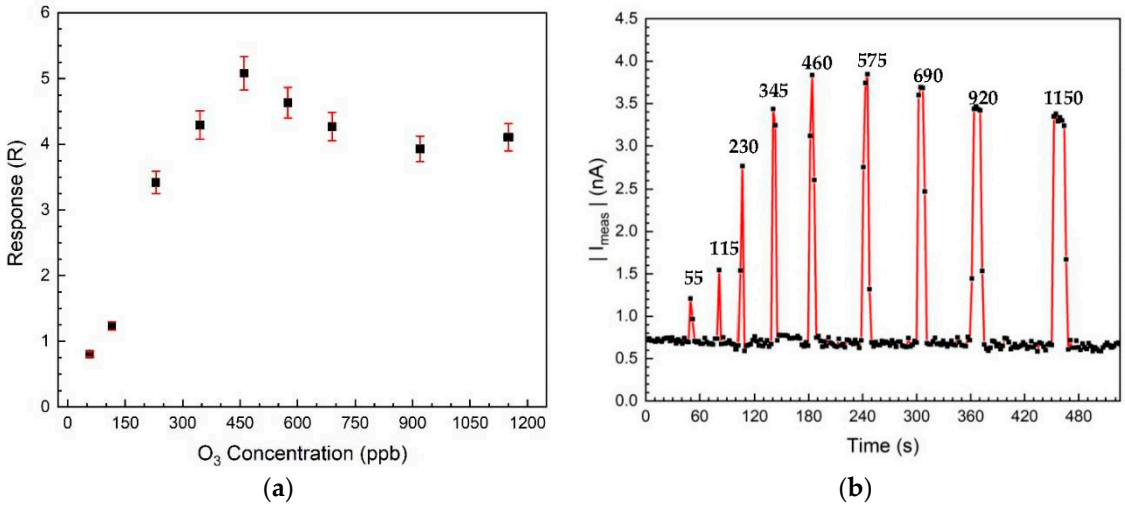

Figure 5. (**a**) Response (R) of the ZnO-based sensor at zero-bias and room temperature as a function of gas concentration. (**b**) Real-time current signal $|I_{meas}|$ recorded without (in air) and with ozone for concentrations of O_3 applied progressively from 55 to 1150 ppb (below each peak is indicated the exact ozone concentration in ppb applied).

As it is possible to see from Figures 5b and 6, the ZnO films tested in this work exhibited a very fast response to the gas concentration (< 2 s) and a good recovery time (< 15 s). However, a decrease in the sensor sensitivity is detected after the exposure of 450 ppb of O3, after that the signal saturation occurs. This behavior could be attributed to two main factors. Firstly, the operations at room temperature may not allow the sensor to fully recondition itself when quickly exposed to gas in close cycles. Secondly, the absorption/desorption mechanisms of the gas and its degradation effects may contribute to reduce the sensor sensitivity. To verify this, an investigation of the surface morphology was performed, revealing significant changes in the nanostructured surface of the ZnO films after the exposure to the pollutants of interest. The action of the gas led to the formation of larger-sized features (up to a few μm) with degradation effects within the formed structures. The surface topographic imaging with nanoscale resolution shown in Figure 7 demonstrates the degradation effects particularly pronounced after O_3 exposure.

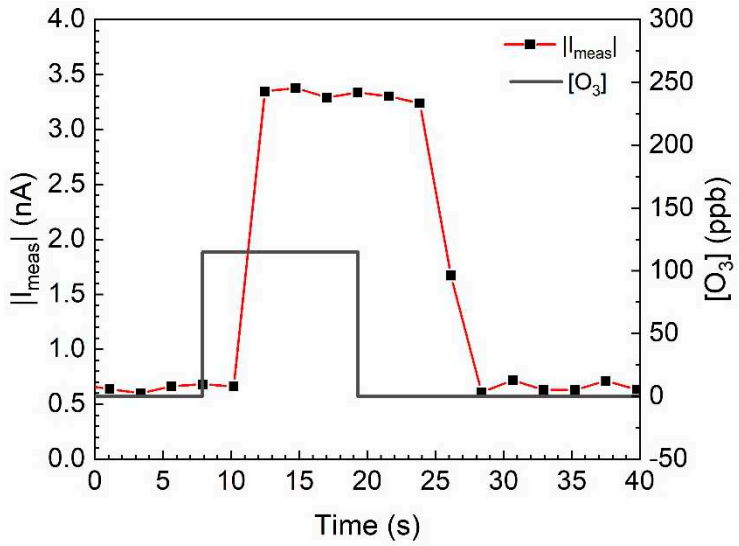

Figure 6. Real-time current $|I_{meas}|$ of the ZnO-based sensor tested at 115 ppb for 10 s with active pumping system.

Preprints (www.preprints.org) | NOT PEER-REVIEWED | Posted: 15 December 2023 doi:10.20944/preprints202312.1121.v1

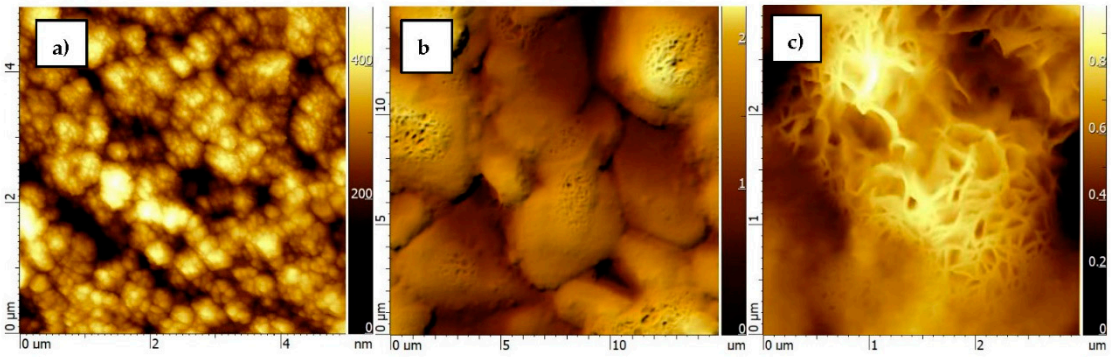

Figure 7. Comparison between AFM images of ZnO deposited on Al_2O_3 before (**a**) and after (**b,c**) O_3 exposure.

Also XPS analysis confirmed the significant effect of degradation on the film surface. The atomic concentration of Zn in the most superficial layer of the film was reduced by more than 80% (from 42.3% to 6.7%) after a massive exposure to O3 gas.

The Raman results after the O3 gas exposure (see Figure 8), for both laser excitation sources, show a signal similar in shape to the unexposed sample (blued solid line), but the main band centered at about 560 cm-1 appears broader, less intense, and shifted by 3 to 10 cm-1 (depending on the observed point). Comparing the Raman measurements with the morphological changes observed form the AFM characterization (see Figure 7) it is possible to suppose that initially the polycrystalline ZnO film is uniformly distributed on the surface of the alumina substrate, in the form of a cubic structure. However, when the film interacts with O3, part of the film is removed leaving uncovered areas of the substrate, while what remains reassembles in the form of ZnO nanowires [34–38]. In other words, it is reasonable to assume that the interaction with the gas modifies the rearrangement of ZnO from small polycrystalline grains to nanowires (and bare areas of alumina) but does not change its chemical nature as a cubic zincblende.

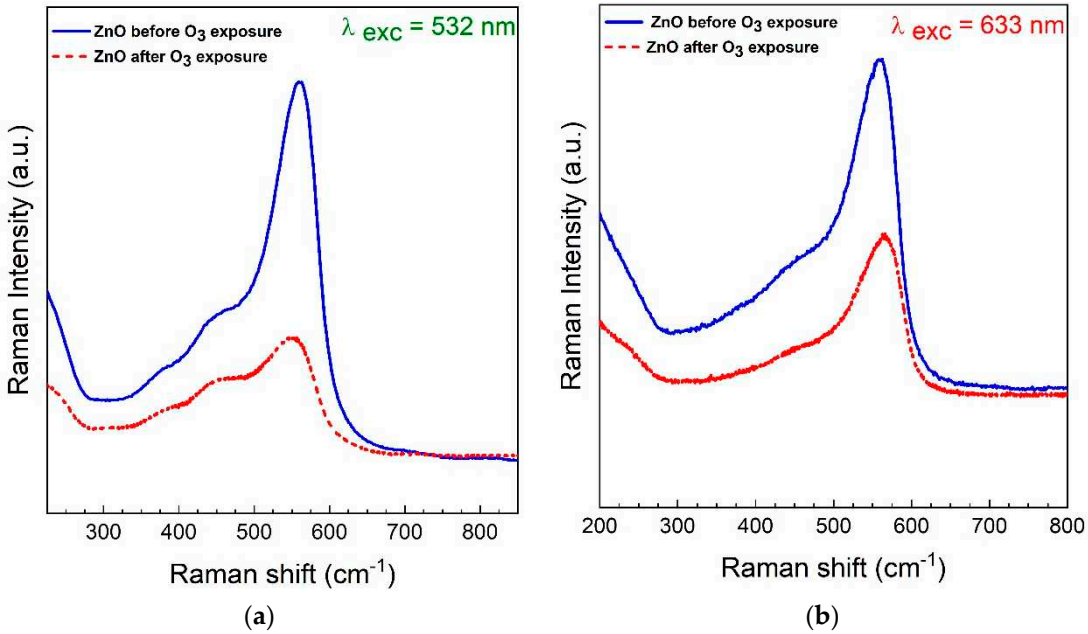

Figure 8. Normalized Raman spectra of ZnO thin film on Al_2O_3 before (solid blue line) and after (dashed red line) exposure to O_3 using λ_{exc} = 532 nm (**a**) and λ_{exc} = 633 nm (**b**) as excitation wavelengths in comparison with ZnO hexagonal wurtzite and Al_2O_3 references. The B1(high) vibration band at ~560 cm^{-1} is due to the presence of cubic structure (cubic zincblende) and nanowires.

What has been deduced from all the analyses is that the degradation effects impact of ozone seems to be irreversible, resulting in the removal of a substantial portion of the film. Despite this, it is notifiable that the ZnO-based sensor still performs well, i.e., the current signal can be clearly discriminated at room temperature and zero-bias, even after exposure to a continuous dose (i.e., the integrated concentration of pollutant during the exposure) of approximately 4500 ppb of ozone. This performance ensures an operational lifespan for the related device exceeding one year (taking into account that the average ozone concentration detected in offices and schools is around 4-6 ppb), making it a favorable compromise for its utilization in such applications. However, further studies to monitor the sensor behavior as a function of time at lower concentrations (< 50 ppb) will be done to confirm the promising performance observed in the measurement range investigated in this work.

4. Conclusions

Ozone sensors based on ZnO thin films have been developed for use at room temperature bias and zero-bias. The grown conditions for achieving better ozone sensitivity performance involve a deposition of 300 nm film through e-beam evaporation on rough alumina substrates. The films with the highest roughness and smallest grain sizes were subjected to ozone sensitivity tests, exhibiting promising results in terms of sensitivity, speed and recovery time. The exposure to ozone leads to the removal of part of the film. Although the surface degradation is irreversible, the sensor application can be for continued monitoring in extended periods (almost one year), making this prototype a promising candidate for low-maintenance applications in schools and offices.

Author Contributions: Conceptualization, A.F., E.B., A.S., and A.B.; methodology, A.F., E.B. and A.B; software, M.M.; validation, A.B. and E.B.; investigation, A.F., A.B., M.M., E.B., V.V., A.M. and R.P.; data curation, E.B. and V.V.; writing—original draft preparation, E.B.; writing—review and editing, E.B., A.B. and D.M.T.; visualization, A.F., A.S., A.B., M.M., E.B., V.V. and R.P.; supervision, D.M.T. All authors have read and agreed to the published version of the manuscript.

Funding: This research was conducted as part of the IBIS ECO "IoT-based Building Information System for Energy Efficiency & Comfort" project ((DGR Basilicata n. 15AB.2021.d.014333, CUP G49J19001400004), funded under the ERDF Operational Program 2014-2020 - Action 1B.1.2.2. "Public Notice" Complex Research and Development Projects "CORES" Thematic Areas "Energy and Bioeconomy".

Acknowledgments: The authors are grateful to Maria Lucia Pace and Enzo Lucia of CNR-ISM U.O.S. Tito Scalo for their administrative support.

References

1. Bassous, N.J.; Rodriguez, A.C.; Leal, C.I.L.; Jung, H.Y.; Lee, C.K.; Joo, S.; Kim, S.; Yun, C.; Hahm, M.G.; Ahn, M.-H.; Kim, S.-W.; Oh, Y.S. and Shin, S.R. Significance of Various Sensing Mechanisms for Detecting Local and Atmospheric Greenhouse Gases: A Review. *Adv. Sensor Res.* **2023**, 2300094. https://doi.org/10.1002/adsr.202300094.
2. Nazaroff, W.W.; Weschler, C.J. Indoor ozone: Concentrations and influencing factors. *Indoor Air*. **2022**, 32:e12942. doi:10.1111/ina.12942.
3. Salonen, H.; Salthammer, T.; Morawska, L. Human exposure to ozone in school and office indoor environments. *Environ. Int*. **2018**, 119: 503-514. https://doi.org/10.1016/j.envint.2018.07.012.
4. Burratti, L.; Bolli, E.; Casalboni, M.; De Matteis, F.; Mochi, F.; Francini, R. et al. Synthesis of Fluorescent Ag Nanoclusters for Sensing and Imaging Applications. *Mater. Sci. Forum*. **2018**, 941:2243–8. https://doi.org/10.4028/www.scientific.net/msf.941.2243.
5. Neri, G. First Fifty Years of Chemoresistive Gas Sensors. *Chemosensors*. **2015**, 3, 1-20. https://doi.org/10.3390/chemosensors3010001.
6. Yoon, J.W.; Grilli, M.L.; Di Bartolomeo, E.; Polini, R and Traversa, E. The NO_2 response of solid electrolyte sensors made using nano-sized $LaFeO_3$ electrodes. *Sens. Actuators B Chem.* **2001,** 76, (1–3): 483-488. https://doi.org/10.1016/S0925-4005(01)00594-9.
7. Chopra K, Kaur I. Thin Film Device Applications. *Springer US*; **1983**.

8. Bellucci, A.; Mastellone, M.; Girolami, M.; Orlando, S.; Medici, L.; Mezzi, A.; Kaciulis, S.; Polini, R.; Trucchi, D.M. ZnSb-based thin films prepared by ns-PLD for thermoelectric applications. *Appl. Surf. Sci.*, **2017**, 418: 589-593.
9. Mezzi, A.; Bolli, E.; Kaciulis, S.; Bellucci, A.; Paci, B.; Generosi, A.; Mastellone, M.; Serpente, V.; Trucchi, D.M. Multi-Technique Approach for Work Function Exploration of Sc2O3 Thin Films. *Nanomaterials*. **2023**, 13, 1430. https://doi.org/10.3390/nano13081430.
10. Hee-Tae Jung. The present and the future of Gas Sensors. *ACS Sensors*. **2022**, 7 (4): 912-913. DOI: 10.1021/acssensors.2c00688.
11. Bochenkov, V. E. and G. B. SergeeV. Sensitivity, Selectivity, and Stability of Gas-Sensitive Metal-Oxide Nanostructures. **2010.**
12. Serpente, V.; Girolami, M.; Mastellone, M.; Sabbatella, G.; Vitulano, A.; Staccioli, M.P.; Riccucci, C.; Di Carlo, G.; Trucchi, D.M. Selective flexible sensor for monitoring volatile organic compounds in museum display cases. *J. Cult. Herit*. **2024**, 66: 1-9. https://doi.org/10.1016/j.culher.2023.10.017.
13. Bogue, R. Emerging applications driving innovations in gas sensing. *Sens. Rev*. **2017**. 37, 2. http://dx.doi.org/10.1108/SR-11-2016-0256.
14. Rose, K.; Eldridge, S. and Chapin, L. The internet of things: An overview. *The internet society (ISOC)*, **2015**, 80: 1-50.
15. Yuan, H.; Aljneibi, S.A.A.A.; Yuan, J.; Wang, Y.; Liu, H.; Fang, J.; Tang, C.; Yan, X.; Cai, H.; Gu, Y.; et al. ZnO nanosheets abundant in oxygen vacancies derived from metal-organic frameworks for ppb-level gas sensing. *Adv. Mater*. **2019**, 31, 1807161.
16. Elger, A.; Hess, C. Elucidating the Mechanism of Working SnO2 Gas Sensors Using Combined Operando UV/Vis, Raman, and IR Spectroscopy. Angew. *Chem. Int. Ed.* **2019**, 58, 15057–15061.
17. Ma, J.; Ren, Y.; Zhou, X.; Liu, L.; Zhu, Y.; Cheng, X.; Xu, P.; Li, X.; Deng, Y.; Zhao, D. Pt nanoparticles sensitized ordered mesoporous WO3 semiconductor: Gas sensing performance and mechanism study. *Adv. Funct. Mater*. **2018**, 28, 1705268.
18. Dey, Ananya. Semiconductor metal oxide gas sensors: A review. *Mater. Sci. Eng. B*. **2018**, 229, 206-217. https://doi.org/10.1016/j.mseb.2017.12.036.
19. Goel, N.; Kunal, K.; Kushwaha, A.; Kuma, M. Metal oxide semiconductors for gas sensing. *Eng. Rep.* **2022**, e12604.
20. Isaac, N.A.; Pikaar, I.; Biskos, G. Metal oxide semiconducting nanomaterials for air quality gas sensors: Operating principles, performance, and synthesis techniques. *Mikrochim Acta*. **2022**, 189, 196.
21. Rescalli, A.; Marzorati, D.; Gelosa, S.; Cellesi, F.; Cerveri, P. Temperature Modulation of MOS Sensors for Enhanced Detection of Volatile Organic Compounds. *Chemosensors*. **2023**, 11, 501. https://doi.org/10.3390/chemosensors11090501.
22. Xue, S.; Cao, S.; Huang, Z.; Yang, D.; Zhang, G. Improving Gas-Sensing Performance Based on MOS Nanomaterials: A Review. *Materials*. **2021**, 14, 4263. https://doi.org/10.3390/ma14154263.
23. Mitra, P.; Chatterjee, A.P.; Maiti, H.S. ZnO thin film sensor. *Mater. Lett*. **1998**, 35 (1–2)1998: 33-38. https://doi.org/10.1016/S0167-577X(97)00215-2.
24. Gaiardo, A.; Fabbri, B.; Giberti, A.; Guidi, V.; Bellutti, P.; Malagù, C.; Valt, M.; Pepponi, G.; Gherardi, S.; Zonta, G.; Martucci, A.; Sturaro, M.; Landini, N. ZnO and Au/ZnO thin films: Room-temperature chemoresistive properties for gas sensing applications. *Sens. Actuators B Chem*. **2016**, 237: 1085-1094. https://doi.org/10.1016/j.snb.2016.07.134.
25. Aydın, H.; Yakuphanoglu, F.; Aydın, C. Al-doped ZnO as a multifunctional nanomaterial: Structural, morphological, optical and low-temperature gas sensing properties. *J. Alloys Compd*. **2019**, 773: 802-811. https://doi.org/10.1016/j.jallcom.2018.09.327.
26. Wang, Z.; Bu, M.; Hu, N.; Zhao, L. An overview on room-temperature chemiresistor gas sensors based on 2D materials: Research status and challenge. *Compos. B. Eng*. **2023**, 248: 110378.
27. Kumar, R.R.; Raja Sekhar, M.; Raghvendra et al. Comparative studies of ZnO thin films grown by electron beam evaporation, pulsed laser and RF sputtering technique for optoelectronics applications. *Appl. Phys. A*. **2020**, 126, 859.
28. Ihokura, K. & Watson, J. The Stannic Oxide Gas Sensor Principles and Applications (1st ed.). *CRC Press*. **1994**. https://doi.org/10.1201/9780203735893
29. Birkefeld, L.D.; Azad, A.M.; Akbar, S.A. Carbon Monoxide and Hydrogen Detection by Anatase Modification of Titanium Dioxide. *J. Am. Ceram. Soc*. **1992**, 75, 2964–2968.

30. Meng, L.J.; de Sá, C.P.M.; Dos Santos, M.P. Study of the structural properties of ZnO thin films by x-ray photoelectron spectroscopy. *Appl. Surf. Sci*. **1994**, 78, 57–61.
31. Manjón, F. J.; Marí, B.; Serrano, J.; Romero, A.H. Silent Raman modes in zinc oxide and related nitrides. *J. Appl. Phys*. **2005**, 97:053516.
32. Wang, Z.; Qiu, X.; Shi, J. and Yu, H. Room Temperature Ozone Detection using ZnO based Film Bulk Acoustic Resonator (FBAR). *Electrochem. Soc.* **2011,** 159 J13. DOI 10.1149/2.054201jes.
33. Takata, M.; Tsubone, D.; Yanagida, H. Dependence of electricalconductivity of ZnO, degree of sensing. J. Am. Ceram. Soc. **1976**, 59, 4–8.
34. Tzolov, M.; Tzenov, N.; Dimova-Malinovska, D.; Kalitzova, M.; Pizzuto, C.; Vitali, G.; Zollo, G.; Ivanov, I. Vibrational properties and structure of undoped and Al-doped ZnO films deposited by RF magnetron sputtering. *Thin Solid Films*. **2000**, 379:28-36.
35. Venkatesh, P.S.; Ramakrishnan, V. and Jeganathan, K. Raman silent modes in vertically aligned undoped ZnO nanorods. *Physica B Condens. Matter*. **2016**, 481, 204-8.
36. Venkatesh, P.S. and Jeganathan, K. Investigations on the growth and characterization of vertically aligned zinc oxide nanowires by radio frequency magnetron sputtering. J. *Solid State Chem*. **2013**, 200: 84–89.
37. Venkatesh, P.S.; Purushothaman, V.; Muthu, S.E.; Arumugam, S.; Ramakrishnan, V.; Jeganathan, K. and Ramamurthi, K. Role of point defects on the enhancement of room temperature ferromagnetism in ZnO nanorods. *Cryst. Eng. Comm*. **2012**, 14: 4713–4718.
38. Ashrafi, A. and Jagadish, C. Review of zincblende ZnO: Stability of metastable ZnO phases. *J. Appl. Phys.* **2007**, 102:071101.